Available online at www.sciencedirect.com

SciVerse ScienceDirect

Energy Procedia 37 (2013) 1584 – 1596

Energy Procedia

GHGT-11

Modeling CO_2 absorption and desorption by aqueous monoethanolamine solution with Aspen rate-based model

Ying Zhang[a], Chau-Chyun Chen[b]*

[a]*AspenTech Limited, Pudong, Shanghai 201203, China*
[b]*Aspen Technology, Inc., Burlington, Massachusetts 01803, U. S. A.*

Abstract

Nineteen data sets of CO_2 absorption by aqueous monoethanolamine solution (0.3g/g monoethanolamine in water) from the recent pilot plant studies at the University of Kaiserslautern have been simulated with Aspen rate-based model. The simulation study was performed with both the rigorous rate-based model and the traditional equilibrium-stage model. The results show the rate-based model yields reasonable predictions on all key performance measurements including CO_2 removal percentage in the absorber, temperature and CO_2 concentration profiles in the absorber and the desorber, and the desorber reboiler duty. In contrast, the equilibrium-stage model fails to reliably predict these key performance variables.

Keywords: CO_2 Capture, Rate-based model, Equilibrium-stage model, aqueous monoethanolamine solution, process simulation

1. Introduction

CO_2 is the major greenhouse gas contributing to the climate change. Over the past few years, there has been much elevated interest in the development of CO_2 capture technologies. Post-combustion CO_2 capture by absorption with chemical solvents is expected to be the dominant technology to reduce CO_2 emission from coal-fired power plants [1]. While this capture technology is being actively investigated for commercial-scale implementation on existing power plants, it is necessary to further reduce the energy penalty, to scale up and optimize the process, and to improve the overall process economics and operability. Rigorous process models are indispensible tools for scientists and engineers to design, scale up, integrate, optimize and operate such post-combustion CO_2 capture units.

In our previous work, we used the rate-based absorption model, RateSep, in Aspen Plus process simulator to simulate the pilot plant at the University of Texas at Austin for CO_2 absorption with aqueous monoethanolamine (MEA) solution [2]. The results show the superiority of the rate-based model over

* Corresponding author. Tel.: 781-221-6420; fax: 781-221-6410.
E-mail address: chauchyun.chen@aspentech.com.

Selection and/or peer-review under responsibility of GHGT
doi:10.1016/j.egypro.2013.06.034

traditional equilibrium-stage models for modeling performance of the CO_2 absorber. For example, the rate-based MEA model accurately predicts CO_2 removal %, CO_2 loading in rich amine, and the temperature profiles observed with the comprehensive pilot plant absorber data sets from University of Texas at Austin. On the contrary, the equilibrium-stage models over-predict CO_2 removal % and CO_2 loading in rich amine, and they are incapable of correctly predicting the absorber temperature profiles.

Recently, a number of new pilot plant studies for CO_2 capture with aqueous MEA solutions have been reported [3-7]. Among them, Mangalapally et al. reported with comprehensive details on the results of a systematic base line study with MEA in a pilot plant at University of Kaiserslautern [3]. In this work, we update the thermodynamic, kinetic, and transport property parameters we used in our prior study [2] and we extend our rate-based simulation study with RateSep to cover both the absorber and the desorber by validating the rate-based MEA model with the comprehensive pilot plant data from Mangalapally et al. [3] Model predictions against the pilot plant data are presented for both the rate-based model and the equilibrium-stage model.

2. MEA model

2.1. Physical properties

Our recent work on thermodynamic representation of the MEA-water-CO_2 system [8] is used in this study. The liquid phase nonideality is accounted for with the electrolyte NRTL activity coefficient model [9]. The solution chemistry for CO_2 absorption with MEA includes water dissociation, CO_2 hydrolysis, bicarbonate dissociation, carbamate hydrolysis, and MEA protonation:

$$2H_2O \leftrightarrow H_3O^+ + OH^- \tag{1}$$

$$CO_2 + 2H_2O \leftrightarrow HCO_3^- + H_3O^+ \tag{2}$$

$$HCO_3^- + H_2O \leftrightarrow CO_3^{-2} + H3O^+ \tag{3}$$

$$MEACOO^- + H_2O \leftrightarrow MEA + HCO_3^- \tag{4}$$

$$MEAH^+ + H_2O \leftrightarrow MEA + H_3O^+ \tag{5}$$

In addition to thermophysical properties, rate-based process models such as RateSep require quantitative models for various transport properties that are essential for correlations of heat transfer, mass transfer, interfacial area, liquid holdup, pressure drop, etc. As summarized previously [2], we have examined the empirical transport property models [10, 11] available in Aspen Plus process simulator and we matched available literature data by adjusting the transport property model parameters for density, viscosity, surface tension, thermal conductivity, and diffusivity. These empirical transport property models provide useful engineering frameworks for data correlation, interpolation and extrapolation.

2.2. Kinetics

We obtain reaction kinetics for carbamate formation from Hikita et al. [12] and for bicarbonate formation from Pinsent et al. [13]. Reactions 6 and 7 are the forward and reverse reactions for carbamate formation, and 8 and 9 are the forward and reverse reactions for bicarbonate formation.

$$MEA + CO_2 + H_2O \rightarrow MEACOO^- + H_3O^+ \quad (6)$$

$$MEACOO^- + H_3O^+ \rightarrow MEA + CO_2 + H_2O \quad (7)$$

$$CO_2 + OH^- \rightarrow HCO_3^- \quad (8)$$

$$HCO_3^- \rightarrow CO_2 + OH^- \quad (9)$$

Table 1 shows the corresponding rate expressions for the forward and backward reactions. Here, k_j is the reaction rate constant for reaction j, K_i is the chemical equilibrium constant for the formation of species i, and a_i is the activity of species i.

Table 1. Kinetic rate expressions considered in the CO_2 capture model

Related Specie	Reaction Direction	Kinetic Expression
$MEACOO^-$	Forward	$r_6 = k_6 * a_{MEA} * a_{CO_2}$ (10)
	Reverse	$r_7 = \frac{k_6}{K_{MEACOO^-}} * \frac{a_{MEACOO^-} * a_{H_3O^+}}{a_{H_2O}}$ (11)
HCO_3^-	Forward	$r_8 = k_8 * a_{CO_2} * a_{OH^-}$ (12)
	Reverse	$r_9 = \frac{k_8}{K_{HCO_3^-}} * a_{HCO_3^-}$ (13)

In Aspen Plus, reaction rates are described by power law expressions:

$$r_j = k_j^0 \exp\left(-\frac{\varepsilon_j}{R}\left[\frac{1}{T} - \frac{1}{298.15}\right]\right)\prod_{i=1}^{N} a_i^{\alpha_{ij}} \quad (14)$$

Here r_j is the reaction rate for reaction j, k_j^0 is the pre-exponential factor, ε_j is the activation energy, R is the gas constant, T is the system temperature in Kelvin, a_i is the activity of species i, and α_{ij} is the reaction order of species i in reaction j. The pre-exponential factor k_j^0 and the activation energy ε_j need to be specified.

The original rate expressions and rate constants obtained from Hikita et al. [12] and Pinsent et al. [13] are in molarity basis. We convert the molarity basis rate constants to activity basis by using the activity coefficients of the reacting species and the density of the solvent. For example, the activity basis rate constant of reaction 6 is calculated by

$$k_6^a = \frac{k_6^{\mathrm{m}} C_{\mathrm{s}}^2}{\gamma_{\mathrm{MEA}} \gamma_{\mathrm{CO_2}}} \quad (15)$$

k^a is the activity basis rate constant, k^m is the molarity basis rate constant, C_s is the molar concentration of the solvent (55.51 kmol/m^3) and γ_i is the activity coefficient of species i.

The parameters for the activity basis rate constants, k_j^0 and ε_j, are shown in Table 2.

Table 2. Constants for power law expressions for the absorption of CO_2 by MEA

Related Species	Reaction Direction	k_j^0 (kmol/m^3.s)	ε_j (kJ/gmol)
$MEACOO^-$	Forward	3.02 x 10^{14}	41.20
	Reverse (absorber)	5.52 x 10^{23}	69.05
	Reverse (desorber)	6.56 x 10^{27}	95.24
HCO_3^-	Forward	1.33 x 10^{17}	55.38
	Reverse	6.63 x 10^{16}	107.24

We calculate the reverse reaction rate constant from the forward reaction rate constant and the equilibrium constant with the following equation:

$$k_r^a = \frac{k_f^a}{K_{eq}} \tag{16}$$

k_f^a is the activity basis rate constant of the forward reaction, k_r^a is the activity basis rate constants of the reverse reaction, K_{eq} is the activity basis equilibrium constant. The logarithms of the rate constant and the equilibrium constant are expressed as a linear function of the reciprocal temperature:

$$\ln k_j(T) = a + \frac{b}{T} \tag{17}$$

$k_j(T)$ is the rate constant or the equilibrium constant at temperature T.

However, the logarithm of the equilibrium constant for the carbamate reaction is not a linear function of the reciprocal temperature in the whole temperature range of interest. To improve the representation of the temperature dependency, we use two linear expressions to approximate the equilibrium constant at low to mid temperatures (303-353 K in the absorber) and at high temperatures (363-393 K in the desorber). Subsequently, as shown in Table 2, we use two different sets of kinetic rate constant parameters for the reverse carbamate reaction for the absorber and the desorber.

3. Pilot plant and process description

The CO_2 absorption/desorption process flowsheet with the pilot plant at the University of Kaiserslautern [3] is reproduced in Figure 1. The main specifications of the pilot plant are summarized in Table 3.

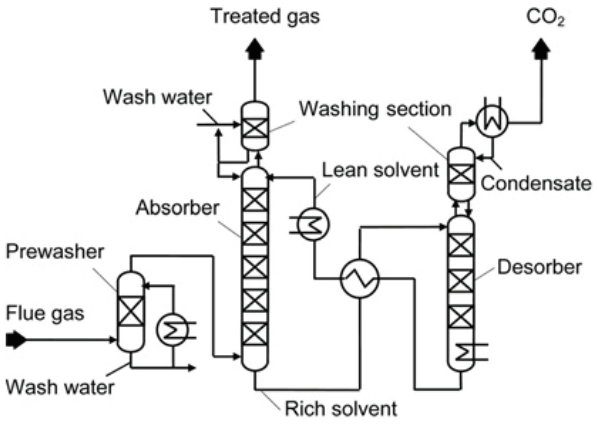

Fig. 1. Flow scheme of the absorption/desorption process [3]

The complete pilot plant and process description is available from Managalapally and Hasse [3]. An abridged summary is given below:

"*The flue gas produced by a gas burner is fed into the pre-washer column by a blower. The pre-washer is built as a direct contact cooler to set the temperature of the flue gas at the absorber inlet and at the same time to make sure that the flue gas is saturated with water. The flue gas enters the absorber at the bottom with a temperature of approximately 40-50 °C. The absorber is built of five sections, which are each equipped with 0.85 m of the structured packing BX 500. The total packing height is 4.25 m. The regenerated solvent (lean solvent) is fed to the absorber top, typically at temperature of 40 °C. Upon the CO_2 absorption into the liquid phase, absorption enthalpy is released, which leads to a temperature increase. To reduce solvent loss by flue gas, there is a washing section at the absorber top above the solvent inlet. A low amount of fresh deionized water is added into the washing water recycle stream to avoid a prohibitive accumulation of amine in the washing water.*

The rich amine is pumped into the desorber through the rich lean heat exchanger, where the CO_2 rich solvent is heated to higher temperatures through the lean solvent from the desorber bottom. The desorber is built of three sections, which are each equipped with five elements of BX 500 similar to the absorber. The total packing height in the desorber is 2.55 m. Both the absorber and desorber column have a diameter of 0.125 m. The bottom of the desorber contains electrical heating elements for partial evaporation of the solvent. For aqueous amine solutions, mainly water is evaporated. The vapor at the top of the desorber consists of water, CO_2 and some traces of amine. To retain the amine, also at the desorber top a washing section is installed. The vapor at the desorber top is led into the condenser where most of the water is removed so that almost pure CO_2 is obtained."

The most important process parameters affecting the capture process are L/G ratio and fluid dynamic load of the absorber (F-factor). Table 4 shows the overall process parameter variation.

Specifically, two series of experiments were carried out with a variation of the L/G ratio (mass ratio, kg/kg): Series A (A1-A6) with the CO_2 partial pressure of 54 mbar in the flue gas, the flue gas flow rate

of 76 kg/hr, and L/G ratio from 0.66 to 2.64; Series B (A7-A12) with the CO_2 partial pressure of 102 mbar in the flue gas, the flue gas flow rate of 80 kg/hr and L/G ratio from 1.56 to 3.5. For both series of experiments removal rate is specified as 90% by adjusting the reboiler duty. Additionally, two series of experiments with a variation of the fluid dynamic load (flue gas flow rate) were carried out: Series C (A15-A17) with a CO_2 partial pressure in the flue gas of 54 mbar, L/G ratio of 1.3, and F-factor from 0.88 to 1.85; Series D (A13-A14, A18-A19) with a CO_2 partial pressure in the flue gas of 102 mbar, L/G ratio of 2.5, and F-factor from 0.88-1.72. Key pilot plant performance results for these 19 cases are summarized in Table 5.

Table 3. Main specifications of pilot plant [3]

Parameter	Data
Flue gas source	Natural gas burner
CO_2 content in the flue gas (vol%) (dry basis)	3-14
Flue gas rate (kg/hr)	30-100
F-factor* in absorber ($Pa^{0.5}$)	0.6-2.1
Solvent flow rate (kg/hr)	20-350
Liquid load in absorber ($m^3/(m^2hr)$)	2-28.5
Inner diameter of pre-washer, absorber, desorber and washing sections (m)	0.125
Type of packing in the absorber and desorber	BX 500
Total height of packing in the absorber (m)	4.25
Total height of packing in the desorber (m)	2.55
Type of packing in the pre-washer and absorber, desorber washing section	Mellapak 250 Y
Total height of packing in the pre-washer (m)	0.84
Total height of packing in the washing sections of the absorber or desorber	0.42

* F-factor is the vapor kinetic energy term defined as the product of gas velocity and square root of gas density.

Table 4. Overview of process parameter variation [3]

Varied parameters	Range of variation
L/G (kg/kg)	0.7-2.5
F-factor ($Pa^{0.5}$)	0.88-1.85

4. RateSep simulation

We set as the simulation input the measured feed conditions of the absorber, i.e., the temperature, pressure, flow rate, and composition of the lean solvent and the flue gas to the absorber. The temperature, flow rate, and composition of the rich solvent and gas from the absorber are calculated as the output. The measured cold-side temperature and pressure of the rich lean heat exchanger are also set as the input. For the desorber, the measured temperature of the condenser and the loading of the lean solvent out of the desorber are set as the input. The temperature, flow rate, and composition of the lean solvent and gas out of the desorber and the heat duty of the reboiler are calculated.

The built-in correlations in Aspen Plus are used to calculate the performance of packing. Specifically, for the structured packing of BX 500, the 1985 correlations of Bravo et al. [14] are used to predict the mass transfer coefficients and the interfacial area. The 1992 correlation of Bravo et al. [15] is used to calculate

the liquid holdup and the Chilton and Colburn correlation [16] is used to calculate the heat transfer coefficients.

RateSep calculates film thickness as the ratio of the average mass transfer coefficient and average diffusivity. It allows several options for modeling film resistance. The "reaction condition" factor, the weighting factor for conditions (temperature and liquid composition) used to calculate reaction rates for the film or for the discretized film segment if the "film discretization" option is chosen, was set to 0.9. The condition is defined as "factor×bulk condition + (1-factor)×interface" condition. A factor of 0 indicates the interface, and a factor of 1 represents the edge of the film next to the bulk. A higher weighting factor means liquid conditions closer to the bulk liquid will carry higher weight. We choose the "film discretization" option and set the number of discretization points for the liquid film to 5, which give six film segments. We set the film discretization ratio to 5, which is the ratio of the thickness of the adjacent discretization regions. A value of film discretization ratio greater than 1 means thinner film regions near the vapor-liquid interface. Furthermore, RateSep provides four different "flow models" to determine the bulk properties used to evaluate the mass and energy fluxes and reaction rates of a stage. The "mixed" flow model is used as the base calculation method. Twenty "mixed" stages are assumed for the packed columns.

It should also be noted that, in the simulations, heat loss of the column is ignored.

5. Results and discussion

5.1. Rate-based simulation results

The rate-based simulation results for the 19 cases are summarized in Table 5, along with the experimental performance data [3].

The values in the "Lean" column in Table 5 are the CO_2 loading (i.e., mole ratios of CO_2/MEA) of the lean solvent that feeds into the top of the absorber. These values are feed stream pilot plant experimental data and they are used directly in simulation. The values in the "Rich" column are the mole ratios of CO_2/MEA of the CO_2 rich solvent, which comes out of the bottom of the absorber and then goes into the top of the desorber. These values are indicative of the performance of the absorber. The values of "CO_2 removal" show the CO_2 removal percentage of the whole absorber/desorber system. The values in the "Energy" column are the reboiler duty of the desorber. These values indicate the performance of the desorber. Giving the absolute average relative errors of 3.3% for the rich loading, 3.3% for the CO_2 removal percentage, and 6.3% for the reboiler duty, the rate-based model predictions for the 19 cases are very satisfactory.

Figures 2-4 show the parity plots of measured and calculated rich loadings, CO_2 removal percentage, and reboiler duty for the 19 cases. Figure 2 shows that the calculated rich loadings are slightly higher than the experimental values at moderate loading but slightly lower than the experimental values at high loading (CO_2 loading > 0.5). Figures 3 and 4 show a roughly even distribution of over- and under-predictions for the CO_2 removal percentage and the reboiler duty, respectively.

Figure 5 shows the reboiler duty, i.e., regeneration energy, as a function of the ratio of the solvent mass flow and flue gas mass flow with two different CO_2 partial pressures in the flue gas: 54 mbar (experiments Series A) and 102 mbar (experiments Series B) and with a constant CO_2 removal rate of

90%. The predictions match the experimental data very well. The results at the high CO_2 partial pressure (102 mbar) given in Figure 5 indicate an optimum L/G ratio of about 2.5 corresponding to regeneration energy of about 4.0 MJ/kg CO_2. With the reduction of CO_2 partial pressure about to its half (54 mbar), the CO_2 mass transferred from flue gas to the solvent is also reduced to about its half. As a result the optimum L/G ratio is also reduced to about its half. The corresponding number of L/G ratio for MEA at the low CO_2 partial pressure is about 1.2 with regeneration energy of about 3.8 MJ/kg CO_2. The rapid rise in the regeneration energy to the left of the optimum L/G ratio is related to the high amount of stripping steam demand. The slow increase in the regeneration energy to the right of the optimum L/G ratio is mainly due to energy requirement to heat up the higher solvent flows.

Table 5. Overall performance

Case	L/G	PCO_2, mbar	Gas flow, kg/hr	Lean	Rich			CO_2 removal, %			Energy, MJ/kg CO_2		
	Exp	Exp	Exp	Exp	Exp	Rate	Equil	Exp	Rate	Equil	Exp	Rate	Equil
A1	0.7	54	76	0.041	0.45	0.475	0.506	81	80	87	10.3	11.5	8.59
A2	1	54	76	0.13	0.448	0.470	0.491	91	94	99	3.72	4.95	3.88
A3	1.3	54	76	0.205	0.465	0.467	0.496	91	88	99	3.76	3.88	3.42
A4	2	54	76	0.259	0.438	0.444	0.461	91	91	99	4.2	4.02	3.67
A5	2.6	54	76	0.25	0.388	0.399	0.408	90	89	100	4.72	4.80	4.45
A6	2.6	54	76	0.276	0.415	0.417	0.432	90	90	100	4.63	4.27	3.82
A7	1.6	102	80	0.087	0.52	0.484	0.533	87	84	94	6.37	6.03	4.09
A8	1.9	102	80	0.131	0.507	0.477	0.512	90	90	99	4.65	4.55	3.51
A9	2.5	102	80	0.205	0.464	0.467	0.494	90	90	99	4.07	3.97	3.55
A10	2.5	102	80	0.186	0.437	0.454	0.469	91	95	100	4.09	4.17	3.80
A11	2.9	102	80	0.212	0.444	0.442	0.455	87	94	99	4.22	4.27	3.98
A12	3.5	102	80	0.23	0.427	0.422	0.433	91	93	99	4.56	4.39	4.07
A13	2.5	102	40	0.23	0.515	0.485	0.520	93	87	98	3.63	3.86	3.37
A14	2.5	102	60	0.208	0.481	0.478	0.502	91	91	99	3.82	3.78	3.42
A15	1.3	54	40	0.222	0.511	0.477	0.512	88	82	93	3.23	3.84	3.37
A16	1.3	54	60	0.204	0.494	0.471	0.500	91	89	99	3.57	3.91	3.46
A17	1.3	54	85	0.203	0.494	0.466	0.502	90	85	96	3.88	3.97	3.45
A18	2.5	102	80	0.308	0.479	0.483	0.526	58	62	77	3.95	3.90	3.16
A19	2.5	102	80	0.233	0.461	0.477	0.531	78	72	87	3.94	3.88	3.17
Absolute average relative error, $\lvert\Delta Y/Y\rvert$ (%)						3.3	5.1		3.3	10.3		6.3	12.5

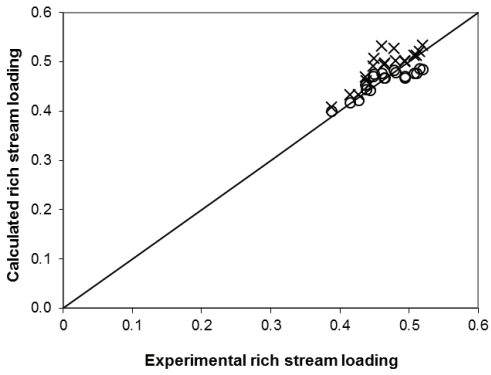

Fig. 2. Parity plot of CO_2 rich loading, (○) results of rate-based method, (×) results of equilibrium-stage method

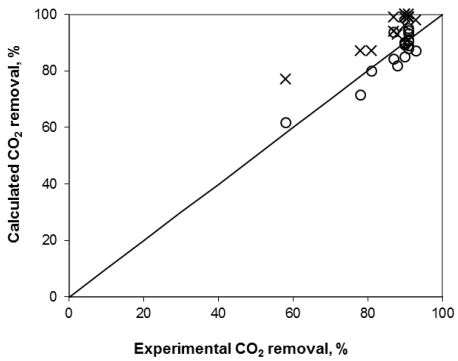

Fig. 3. Parity plot of CO_2 removal percentage, (○) results of rate-based method, (×) results of equilibrium-stage method

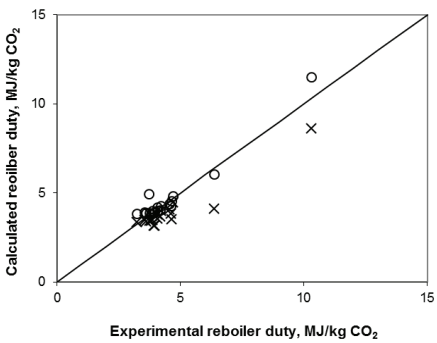

Fig. 4. Parity plot of reboiler duty, (○) results of rate-based method, (×) results of equilibrium-stage method

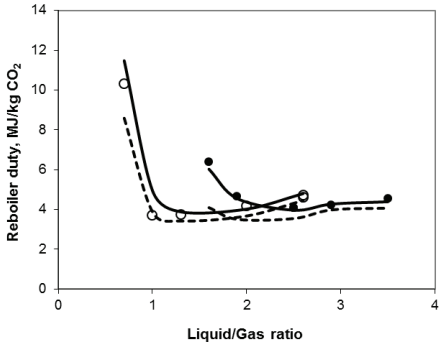

Fig. 5. Comparison of the experimental data (symbols) for reboiler duty and the model results (lines) respect to the ratio of solvent mass flow to flue gas mass flow (liquid/gas ratio), (○) low CO_2 partial pressure (around 54 mbar) in flue gas, (●) high CO2 partial pressure (around 102 mbar) in flue gas, (—) results of rate-based method, (----) results of equilibrium-stage method

5.2. Comparison of rate-based model and equilibrium-stage model

To validate the superiority of the rate-based simulation over the traditional equilibrium-stage simulation, we perform equilibrium-stage simulation for all 19 cases shown in Table 5. In performing the equilibrium-stage simulation, we assume 25 equilibrium stages for both the absorber and the desorber. Equilibrium stage number of 25 is the average of the equilibrium stage numbers of all the 19 cases which we estimate from the packing heights of the absorber and desorber and the results of HETP obtained from the rate-based simulation. In addition, we assume chemical equilibrium conditions for all liquid phase reactions with the equilibrium-stage simulation. The equilibrium-stage simulation yields the absolute average relative errors of 5.1% for the rich loading, 10.3% for the CO_2 removal percentage, and 12.5% for the reboiler duty. The equilibrium-stage simulation results are considerably inferior to the rate-based simulation results. We also found that variations in the equilibrium stage number (above 20 equilibrium stages) with the equilibrium-stage simulation do not significantly alter the simulation results because the equilibrium limit is approached. For example, the reboiler duty of Case A1 only decreases from 8.62 MJ/kg CO_2 to 8.59 MJ/kg CO_2 when the equilibrium stage numbers of both absorber and desorber are changed from 20 to 25; the CO_2 removal percent and the CO_2 loading in the rich amine leaving the absorber remains 87 % and 0.506, respectively.

Figures 2-4 show the parity plots of measured and calculated rich loadings, CO_2 removal percentage, and reboiler duty for the 19 cases. Figure 2 shows that the rich loadings calculated from the equilibrium-stage simulation are always higher than the experimental values. Figure 3 shows over-predictions for the CO_2 removal percentage. Figure 4 shows under-predictions for the reboiler duty.

Figure 5 shows the calculated desorber reboiler duties from the equilibrium-stage simulation are consistently lower than the results of the rate-based simulation and the experimental data. For example, the measured reboiler duty of Case A3 is 3.76 MJ/kg and the result of the rate-based simulation is 3.88 MJ/kg, compared to 3.42 MJ/kg from the equilibrium-stage simulation. The reason is that the equilibrium-stage simulation over-estimates the CO_2 loading in the rich amine and that leads to under-estimation of the reboiler duty per kg CO_2. Note that we choose A3 as an example because it is an optimum case with the minimum regeneration energy.

Figure 6 shows the experimental temperature and CO_2 concentration (in liquid phase) profiles of absorber in Case A3. The simulation results of the rate-based MEA model and the equilibrium-stage model are also given. Consistent with our earlier finding [2], Figure 6 shows the predictions of the rate-based model match the experimental absorber temperature and CO_2 concentration profiles very well while those of the equilibrium-stage model deviate completely from the observed pilot plant data. The experimental data and the rate-based simulation show that CO_2 are absorbed evenly in the whole absorber and both the temperature and CO_2 concentration change gradually along the column. To the contrary, the equilibrium-stage model over-estimates the CO_2 absorption rate and suggests CO_2 absorption and temperature bulge taking place near the bottom. The equilibrium-stage model also significantly over-estimates the CO_2 loading of 0.496 in the rich amine at the bottom of the absorber, compared to the experimental value of 0.465 and the rate-based simulation result of 0.467.

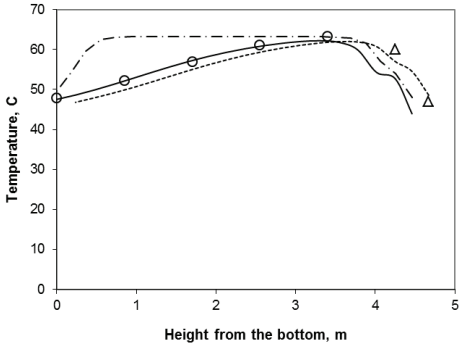

(a)

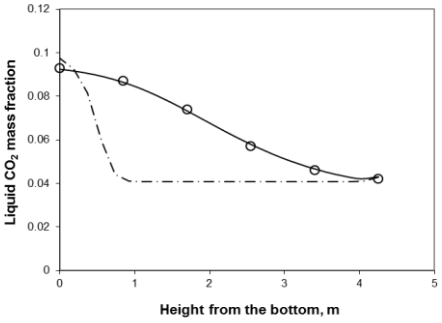

(b)

Fig. 6. Absorber (a) temperature and (b) CO_2 concentration (in liquid phase) profile for Case A3, experimental data (symbols) and simulation results (lines), (a) (○) liquid temperature, (△) gas temperature, (—) liquid temperature predicted by rate-based simulation, (----) gas temperature predicted by rate-based simulation, (— · — ·) temperature predicted by equilibrium-stage simulation, (b) (○) liquid CO_2 concentration, (—) CO_2 concentration predicted by rate-based simulation, (— · — ·) CO_2 concentration predicted by equilibrium-stage simulation

Figure 7 shows, for the desorber, both the rate-based simulation and the equilibrium-stage simulation give reasonable results for the temperature profile while the predictions for CO_2 concentration profile are slightly lower than the experimental data near the top. The CO_2 concentrations in the liquid leaving the feed stage calculated by both rate-based simulation and equilibrium-stage simulation are around 0.080 g/g solution, while the measured value is 0.085 g/g solution. Considering that the liquid CO_2 concentration of the rich amine from the absorber calculated by the rate-based simulation is 0.092 g/g solution, the experimental value is 0.093 g/g solution, and that of the equilibrium-stage simulation is 0.097 g/g solution, we conclude the rate-based simulation results are reliable.

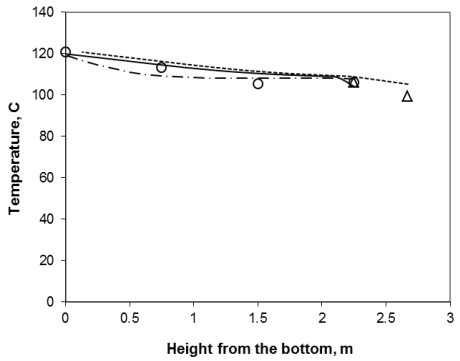

(a)

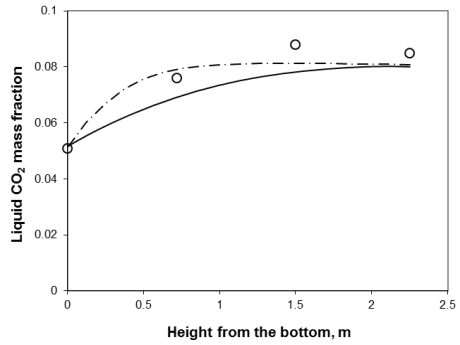

(b)

Fig. 7. Desorber (a) temperature and (b) CO_2 concentration (in liquid phase) profiles for Case A3, experimental data (symbols) and simulation results (lines), (a) (○) liquid temperature, (△) gas temperature, (—) liquid temperature predicted by rate-based simulation, (----) gas temperature predicted by rate-based simulation; (— · — ·) temperature predicted by equilibrium stage simulation; (b) (○) liquid CO2 concentration, (—) CO2 concentration predicted by rate-based simulation, (— · — ·) CO2 concentration predicted by equilibrium stage simulation

In summary, the equilibrium-stage simulation cannot give reliable temperature and concentration profiles for the absorber, may over-estimate the CO_2 absorption, and significantly under-estimate the desorber reboiler duty per unit mass of CO_2.

6. Conclusion

We extend our rate-based simulation model for CO_2 absorption with MEA to the whole absorption/desorption system and we validate the model with the recently published pilot plant data from the University of Kaiserslautern [3] for CO_2 capture with aqueous monoethanolamine. The rate-based model provides excellent predictions for the overall performance of the CO_2 capture system, including CO_2 removal percentage, CO_2 loading, reboiler duty, etc. while the equilibrium-stage model cannot predict these key performance variables reliably. The rate-based model should be a very useful simulation and optimization tool for engineers to study sensitivities of various CO_2 capture process variables, including liquid/gas ratio, CO_2 concentration in the feed stream, CO_2 loading and MEA concentration in the lean amine stream, operating pressure, packing height and type, etc.

References

[1] Rochelle GT. Amine scrubbing for CO_2 capture. *Science*, 2009; 325:1652-1654.

[2] Zhang Y, Chen H, Chen C-C, Plaza JM, Dugas R, Rochelle GT. Rate-based process modeling study of CO_2 capture with aqueous monoethanolamine solution. *Ind. Eng. Chem. Res.*, 2009; 48:9233-9246.

[3] Mangalapally HP, Hasse H. Pilot plant study of post-combustion carbon dioxide capture by reactive absorption: methodology, comparison of different structured packings, and comprehensive results for monoethanolamine. *Chemical Engineering Research and Design*, 2011; 89:1216-1228.

[4] Tobiesen FA, Juliussen O, Svendsen HF. Experimental validation of a rigorous absorber model for CO_2 postcombustion capture. *AIChE Journal*, 2007; 53:846-865.

[5] Tobiesen FA, Juliussen O, Svendsen HF. Experimental validation of a rigorous desorber model for CO_2 postcombustion capture. *Chemical Engineering Science*, 2008; 63:2641-2656.

[6] Knudsen JN, Jensen JN, Vihelmsen PJ, Biede O. Experience with CO_2 capture from coal flue gas in pilot-scale: testing of different amine solvents. *Energy Procedia*, 2009; 1:783-790.

[7] Mangalapally HP, Notz R, Hoch S, Asprion N, Sieder G, Garcia H, Hasse H. Pilot plant experimental studies of post-combustion CO_2 capture by reactive absorption with MEA and new solvents. *Energy Procedia*, 2009; 1:963-970.

[8] Zhang Y, Que H, Chen C–C. Thermodynamic modeling for CO_2 absorption in aqueous MEA solution with electrolyte NRTL model. *Fluid Phase Equilibria*, 2011; 311:68-76

[9] Song YA, Chen C-C. Symmetric electrolyte nonrandom two-liquid activity coefficient model, *Ind. Eng. Chem. Res.*, 2009; 48:7788-7797

[10] Aspen Technology Inc. *Aspen Plus online documentation*, 2008.

[11] Aspen Technology Inc. *Aspen properties reference manual*, Burlington, MA: Aspen Technology Inc.; 2006

[12] Hikita H, Asai S, Ishikawa H, Honda M. The kinetics of reactions of carbon dioxide with monoethanolamine, diethanolamine, and triethanolamine by a rapid mixing method, *Chem. Eng. J.*, 1977; 13:7-12

[13] Pinsent BR, Pearson L, Roughton FJW. The kinetics of combination of carbon dioxide with hydroxide ions, *Trans. Faraday Soc.*, 1956; 52:1512-1520

[14] Fair JR, Bravo JL. Prediction of mass transfer efficiencies and pressure drop for structured tower packings in vapor/liquid service. *Inst. Chem. Eng. Symp. Ser.*, 1987; 104:A183-200

[15] Bravo JL, Rocha JA, Fair JR. Comprehensive model for the performance of columns containing structured packings. *Inst. Chem. Eng. Symp. Ser.*, 1992; 129:A439-457

[16] Taylor R, Krishna R. *Multicomponent Mass Transfer*, New York: John Wiley & Sons, Inc.; 1993